Time dependent density functional theory study of charge-transfer and intramolecular electronic excitations in acetone–water systems

Bernasconi, L ; Sprik, M ; Hutter, J

Abstract: A recently introduced formulation of time dependent linear response density functional theory within the plane-wave pseudopotential framework [J. Hutter, J. Chem. Phys. 118, 3928 (2003)] is applied to the study of solvent shift and intensity enhancement effects of the (1)A(2) n–>pi* electronic transition in acetone, treating solute and solvent at the same level of theory. We propose a suitable formalism for computing transition intensities based on the modern theory of polarization, which is applicable to condensed-phase and finite systems alike. The gain in intensity brought about by thermal fluctuations is studied in molecular acetone at room temperature, and in gas-phase (CH3)(2)CO.(H2O)(2) at 25 K. The latter system is characterized by the appearance of relatively intense features in the low-energy region of the spectrum, attributable to spurious solvent–>solute charge-transfer excitations created by deficiencies in the DFT methodology. The n–>pi* transition can be partially isolated from the charge-transfer bands, yielding a blueshift of 0.17 eV with respect to gas-phase acetone. This analysis is then carried over to a solution of acetone in water, where further complications are encountered in the from of a solute–>solvent charge transfer excitations overlapping with the n–>pi* band. The optically active occupied states are found to be largely localized on either solute or solvent, and using this feature we were again able to isolate the physical n–>pi* band and compute the solvatochromic shift. The result of 0.19 eV is in good agreement with experiment, as is the general increase in the mean oscillator strength of the transition. The unphysical charge transfers are interpreted in terms of degeneracies in the spectrum of orbital energies of the aqueous acetone solution.

DOI: https://doi.org/10.1063/1.1625633

Time dependent density functional theory study of charge-transfer and intramolecular electronic excitations in acetone–water systems

Leonardo Bernasconi and Michiel Sprik
Department of Chemistry, University of Cambridge, Lensfield Road, Cambridge CB2 1EW, United Kingdom

Jürg Hutter
Physical Chemistry Institute, University of Zurich, Winterthurerstrasse, 190, CH-8057 Zurich, Switzerland

(Received 25 August 2003; accepted 22 September 2003)

A recently introduced formulation of time dependent linear response density functional theory within the plane-wave pseudopotential framework [J. Hutter, J. Chem. Phys. **118**, 3928 (2003)] is applied to the study of solvent shift and intensity enhancement effects of the $^1A_2\ n\rightarrow\pi^*$ electronic transition in acetone, treating solute and solvent at the same level of theory. We propose a suitable formalism for computing transition intensities based on the modern theory of polarization, which is applicable to condensed-phase and finite systems alike. The gain in intensity brought about by thermal fluctuations is studied in molecular acetone at room temperature, and in gas-phase $(CH_3)_2CO\cdot(H_2O)_2$ at 25 K. The latter system is characterized by the appearance of relatively intense features in the low-energy region of the spectrum, attributable to spurious solvent $\rightarrow$solute charge-transfer excitations created by deficiencies in the DFT methodology. The $n\rightarrow\pi^*$ transition can be partially isolated from the charge-transfer bands, yielding a blueshift of 0.17 eV with respect to gas-phase acetone. This analysis is then carried over to a solution of acetone in water, where further complications are encountered in the from of a solute$\rightarrow$solvent charge transfer excitations overlapping with the $n\rightarrow\pi^*$ band. The optically active occupied states are found to be largely localized on either solute or solvent, and using this feature we were again able to isolate the physical $n\rightarrow\pi^*$ band and compute the solvatochromic shift. The result of 0.19 eV is in good agreement with experiment, as is the general increase in the mean oscillator strength of the transition. The unphysical charge transfers are interpreted in terms of degeneracies in the spectrum of orbital energies of the aqueous acetone solution. © *2003 American Institute of Physics.*
[DOI: 10.1063/1.1625633]

I. INTRODUCTION

Time dependent density functional theory (TDDFT) (Refs. 1 and 2) is rapidly coming to prominence in the field of computational quantum chemistry as a viable and affordable tool for estimating vertical excitation energies of molecular systems, and several implementations have been described during the last decade based on localized orbital basis sets.[3–9] In principle, the TDDFT method can also be applied using plane-wave pseudopotential techniques.[10] However, only recently, has an efficient perturbative formulation of TDDFT been proposed[11] which makes such calculations feasible for larger systems. Several desirable features, including orthogonality, independence of nuclear positions, absence of basis set superposition errors, make plane-waves an attractive alternative to localized basis sets in several problems of physical and chemical interest. In addition, the extended Lagrangian formalism of Car and Parrinello[12,13] is most naturally implemented using plane-waves, which allows to study the relative importance of thermal relaxation and fluctuation on the absorption profile due to electronic excitations in molecules,[10] and to perform geometry optimizations and, possibly, molecular dynamics simulations on molecules in their excited states.[11] Together with the recent attempts based on TDDFT at computing several properties of excited states of molecular systems directly available from experiment,[14–17] these latest developments may pave the way for a complete and accurate characterization of excited state surfaces, which is of paramount importance in predicting fluorescence spectra and in elucidating the nature of electron transfers in photochemical reactions.

The application of TDDFT to condensed phase systems is also emerging as a very active and multifaceted field of research[18–20] (for a review and further references see Ref. 21). A major advantage of TDDFT for the solid state, is that it potentially offers a rather inexpensive alternative to many-body Green's function methods, relative ease of implementation within conventional Kohn–Sham density functional theory codes, and the possibility to improve progressively, and possibly systematically, the accuracy of the results through increasingly sophisticated representations of the changes in the exchange and correlation interactions between electrons brought about by the excitation. Moreover, TDDFT is often also capable of providing ways to interpret the excitation process in terms of the underlying one-particle picture which is implicit in the Kohn–Sham representation of the ground state. This may be of particular relevance whenever insight from finite size chemical systems (e.g., molecules in the gas phase) can be useful in interpreting specific features of confined systems embedded in a condensed phase environment, like defects or impurities in solids or molecules in

solution. Plane-wave basis sets are again particularly well suited to represent efficiently the charge density distribution in extended systems and they apply naturally to systems obeying periodic boundary conditions.[13]

An important element in the extension of TDDFT calculations to large systems, is the use of relatively simple exchange correlation functionals, such as the various versions of the generalized gradient approximation (GGA) which have been developed for ground state properties. While TDDFT implementations based on GGA's have been successful in describing valence excitations of single molecules, applications to polar molecules, dimers or molecules with stretched bonds have revealed a number of serious problems. In particular the transition frequencies of excitations involving charge transfer are badly underestimated[22–24] and exhibit a qualitatively incorrect dependence on intermolecular distance.[24] More serious perhaps are the difficulties encountered in TDDFT treatments of excitations of biradical systems created by homolytic bond breaking or twisting of double bonds.[25,26] It is an interesting question to what extent these complications are transferred to, and amplified by, the condensed phase. Indeed, the first applications to extended systems (solids, polyenes) have exposed a number of limitations. Approximations, which proved adequate for calculation of spectral properties of finite molecules, were found to give rise to major discrepancies in the larger systems. For example, while for small molecules (or functional groups) the corrections to the bare Kohn–Sham excitations can be substantial, there is little or no improvement for the band gaps in solids.[21] In special cases, the response kernels commonly employed in static and time dependent calculations can produce rather pathological behavior. A notorious example is the huge overestimation of the hyperpolarizability of polyenes.[27–29]

In this paper we investigate the performance of TDDFT for a molecular system in solution, namely aqueous acetone. This system has played the role of benchmark model for the computation of solvatochromic effects and has been the subject of numerous investigations using continuum solvation methods[30–34] or mixed quantum mechanics/molecular mechanics (QM/MM) techniques.[35,36] Molecular solutions appear to be a separate class of condensed systems, occupying a position intermediate between, on the one hand, isolated optically active molecules in vacuum and, on the other hand, semiconductors or polyenes. Solutions are extended systems, but still consist of finite molecular units with optical spectra dominated by localized excitations. Indeed, the ≈ 0.2 eV blue shift of the $n \rightarrow \pi^*$ transition of acetone in response to solvation in water can be understood and quantitatively reproduced at the level of a QM/MM calculation in which all solvent molecules (including the molecules directly hydrogen bonded to the carbonyl group) are treated classically, as has been shown in a previous publication.[36] In the present study we return to this system but this time using a full quantum mechanical description of both solute *and* solvent. The primary aim of this calculation is to analyze in detail the effect of mixing of solvent and solute states as manifested in the vibronic enhancements of transition intensities.[37] To this end we start with an outline of a novel scheme for the computation of the dipole oscillator strength based on an extension of the modern theory of polarization[38–43] to the nonadiabatic regime. We will show that such an unbiased description of solute and solvent is beset by complications related to the collective nature of the electronic states, which are circumvented in the QM/MM approach. This includes spurious charge transfer excitations between solvent and solute and entanglement with the onset of solvent→solvent excitations, which as a result of the serious underestimation of the band gap in Kohn–Sham calculations extend down to far too low energies in calculated TDDFT spectra. A second objective of this paper is, therefore, to identify these effects and place them in the wider context of the ongoing development of density functionals.

After a brief introduction to the electronic spectroscopy of aqueous acetone, listing some of the relevant literature (Sec. II), we summarize in Sec. III the theoretical background of the TDDFT implementation used in this work. A more thorough description of the method can be found in Ref. 11 and detailed discussions of its theoretical foundations in Refs. 2 and 3. In addition, we introduce our scheme for computing oscillator strength in condensed-phase systems and briefly address the problem of transition assignments, which were not treated in Ref. 11. Technical details of the calculations are presented in Sec. IV. The influence of thermal relaxation effects on the intensity of the $n \rightarrow \pi^*$ transition in gas-phase acetone is studied in Sec. V. This analysis is then carried over to the gas-phase $(CH_3)_2CO \cdot (H_2O)_2$ complex, in the optimized geometry and at $T = 25$ K and to the full acetone–water solution. Section VI contains the summary and conclusions.

II. ELECTRONIC SPECTROSCOPY OF AQUEOUS ACETONE

The $n \rightarrow \pi^*$ transition in acetone corresponds to the promotion of one electron from the lone-pair to the antibonding π^* orbital of the C–O group. The $^1A_2$ excitation is symmetry forbidden and the observation of a weak band (oscillator strength $f \simeq 4 \times 10^{-4}$) at ~ 4.5 eV (Refs. 44–47) in the gas-phase is attributed to vibronic coupling and intensity borrowing mechanisms. In water solution the transition can also become allowed, owing to the formation of water–acetone complexes, which may break the C_{2v} symmetry of the molecule. The charge delocalization from the oxygen to the carbonyl carbon brought about by the excitation process reduces the molecular dipole moment and elongates the C–O bond.[48] A large blueshift of the transition energy is observed, ranging from 0.19 (Ref. 49) to 0.21 eV,[50–52] explained by the selective solvent stabilization of the ground state. This is accompanied by an increase in the oscillator strength of $\sim 50\%$ compared to the gas-phase molecule.

Ab initio calculations on small acetone–water clusters have been used as convenient means to study the blueshift and intensity enhancement effects induced by water coordination. Liao *et al.*[53] presented thorough results on the structure and stability of several $(CH_3)_2CO \cdot (H_2O)_n$ $(n = 1-3)$ complexes in the gas phase. Density functional theory (B3LYP) and high-level *ab initio* methods [MP2, CCSD(T)] were used to characterize their structure and energetics and

to compute vibrational spectra. The excitation energies and oscillator strengths for the $n \rightarrow \pi^*$ transition were estimated using CIS, CASSCF, and CASPT2. A blueshift of the excitation energy was computed of 0.1–0.4 eV, depending on the number of coordinated water molecules and cluster geometry, and the oscillator strength was shown to increase from zero to $\sim 10^{-4}$ in $(CH_3)_2CO \cdot (H_2O)_3$. Vibronic coupling was found to be the main mechanism responsible for the increase in spectral intensities, compared to orbital mixing resulting from the water molecule coordination. More recently Röhrig *et al.*[36] investigated the acetone–water solution using a mixed QM/MM Car–Parrinello scheme in which the solvent was treated purely classically. The excited state potential energy surface was described using both TDDFT methods and the restricted open shell Kohn–Sham formalism..[54] They were able to reproduce the experimental solvent shift in passing from the gas-phase molecule to the condensed phase to good accuracy and thus verify that the dominant mechanism responsible for the solvatochromic shift in solution consists of selective electrostatic stabilization of the ground state relative to the excited state.

III. THEORY AND METHOD

A. The dipole approximation in DFT

The fundamental Hamiltonian for a system of electrons in the presence of a time dependent vector potential $\mathbf{A}(\mathbf{r},t)$ and scalar potential $\Phi(\mathbf{r},t)$ is given by

$$H=\frac{1}{2m}\sum_i \left(\mathbf{p}_i+\frac{e}{c}\mathbf{A}(\mathbf{r}_i,t)\right)^2+\sum_{i,I} V_I(\mathbf{r}_i-\mathbf{R}_I) + \frac{1}{2}\sum_{i,j}\frac{e^2}{|\mathbf{r}_i-\mathbf{r}_j|}-\sum_i e\Phi(\mathbf{r}_i,t), \tag{1}$$

where, in the usual notation, c is the velocity of light, $-e$ is the charge of an electron, and m its mass. The one-electron potential $V_I(\mathbf{r}_i-\mathbf{R}_I)$ represents the interaction with the nucleus I at position $\mathbf{R}_I$. The Hamiltonian of Eq. (1) is derived assuming the Coulomb gauge ($\nabla \cdot \mathbf{A}=0$) (see e.g. Ref. 55) and is often referred to as the minimal coupling Hamiltonian. In this gauge the scalar potential $\Phi(\mathbf{r},t)$ describes the longitudinal component $\mathbf{E}_L=-\nabla\Phi$ of the electric field, and is therefore zero in the transversal radiation fields of interest here. The transversal component of the electric field is obtained from the vector potential

$$\mathbf{E}_T=-\frac{\dot{\mathbf{A}}}{c}, \tag{2}$$

where the dot denotes a derivative with respect to time.

In time dependent density functional applications, the minimal coupling Hamiltonian is converted to an energy functional. We will use the functional

$$E=T+\frac{e^2}{2}\int d\mathbf{r}d\mathbf{r}'\frac{n(\mathbf{r},t)n(\mathbf{r}',t)}{|\mathbf{r}-\mathbf{r}'|}+\int d\mathbf{r} n(\mathbf{r},t) \times\left(\sum_I V_I(\mathbf{r}-\mathbf{R}_I)-e\Phi(\mathbf{r},t)\right)+E_{\mathrm{xc}}[n(\mathbf{r},t)], \tag{3}$$

where $n(\mathbf{r},t)$ is the time dependent density which is related to the orbitals as

$$n(\mathbf{r},t)=2\sum_{n=1}^{\mathrm{occ}}\phi_n^*(\mathbf{r},t)\phi_n(\mathbf{r},t), \tag{4}$$

where summation is over occupied orbitals and we have assumed a spin-restricted approach. As in the majority of TDDFT studies (see however Ref. 19) we have adopted the adiabatic local density approximation (ALDA) (Ref. 4) setting the exchange correlation action functional of TDDFT equal to the static exchange-correlation energy functional E_{xc} used in the ground state calculation. Moreover, also coupling to currents is neglected, and the kinetic energy term reduces to

$$T=\frac{1}{m}\sum_{n=1}^{\mathrm{occ}}\langle\phi_n(t)|\left(\mathbf{p}+\frac{e}{c}\mathbf{A}(\mathbf{r},t)\right)^2|\phi_n(t)\rangle, \tag{5}$$

where $\mathbf{A}(\mathbf{r},t)$ is the external vector potential (for the generalization to current density functional theory, see Ref. 56).

If we are only interested in the linear response, the kinetic energy functional can be expanded to first order in the vector potential

$$T=\frac{1}{m}\sum_{n=1}^{\mathrm{occ}}\langle\phi_n(t)|\mathbf{p}^2|\phi_n(t)\rangle+\frac{e}{mc}\sum_{n=1}^{\mathrm{occ}}\langle\phi_n(t)|\mathbf{p}\cdot\mathbf{A}(\mathbf{r},t) + \mathbf{A}(\mathbf{r},t)\cdot\mathbf{p}|\phi_n(t)\rangle. \tag{6}$$

The first term is the kinetic energy in zero field. Thus, substituting back in Eq. (3) we see that we can express the total energy in perturbative form

$$E=E_0+E_{\mathrm{int}}, \tag{7}$$

where E_0 is the energy functional in zero field. The interaction term E_{int} is given by

$$E_{\mathrm{int}}=\frac{2e}{mc}\sum_{n=1}^{\mathrm{occ}}\langle\phi_n(t)|\mathbf{p}\cdot\mathbf{A}(\mathbf{r},t)|\phi_n(t)\rangle - e\int d\mathbf{r}\, n(\mathbf{r},t)\Phi(\mathbf{r},t), \tag{8}$$

where we have used that in the Coulomb gauge the vector field and momentum operator commute ($\mathbf{p}\cdot\mathbf{A}-\mathbf{A}\cdot\mathbf{p}=-i\hbar\nabla\cdot\mathbf{A}=0$).

The interaction functional of Eq. (8), with the scalar potential $\Phi=0$, is the basis for linear response calculations of the electronic spectra in DFT. The derivation is completely standard. The reason we have summarized it here is to be able to continue with the next step, the introduction of the dipole approximation for molecular systems. This is usually implemented at the level of the Hamiltonian Eq. (1) using a gauge transformation involving the polarization operator.[55] However, as the modern theory of polarization has demonstrated,[40] polarization in periodic systems cannot be represented as the expectation value of a Hermitian operator and the Hamiltonian route is not an option. Fortunately, in the simple case of the dipole coupling, it is possible to directly apply a suitable gauge transformation to the energy functional Eq. (8), as we will now show.

In this derivation the long wave length limit is introduced at the start, ignoring spatial dependence of **A**. This also eliminates magnetic effects since the magnetic component of the radiation field $\mathbf{B}=\nabla\times\mathbf{A}$ vanishes. Next we define the gauge function

$$\Xi(t)=-\frac{L^3}{Ne}\mathbf{A}(t)\cdot\mathbf{P}(t), \tag{9}$$

where $\mathbf{A}(t)$ is the uniform vector potential and L^3 the volume of the cubic supercell. $\mathbf{P}(t)$ the expectation value of the polarization. If the system can be partitioned in nonoverlapping molecular charge distributions (Clausius–Mossotti limit) we can express polarization as a sum of dipole moments.

$$\mathbf{P}(t)=-\frac{e}{L^3}\int d\mathbf{r}\;\; n(\mathbf{r},t)\mathbf{r}. \tag{10}$$

Vector potentials transform, under a change of gauge, according to

$$\tilde{\mathbf{A}}(\mathbf{r},t)=\mathbf{A}(\mathbf{r},t)-\nabla\,\Xi(\mathbf{r},t). \tag{11}$$

Hence, in the long wavelength approximation, **A** is invariant, since the gauge function Ξ of Eq. (9) is constant over space. The scalar potential in the new gauge becomes finite

$$\tilde{\Phi}(\mathbf{r},t)=\Phi(\mathbf{r},t)+\frac{1}{c}\dot{\Xi}(\mathbf{r},t)=-\frac{L^3}{Nec}(\dot{\mathbf{A}}\cdot\mathbf{P}+\mathbf{A}\cdot\dot{\mathbf{P}}). \tag{12}$$

Integrating over charge density and substituting in Eq. (8) we find

$$E_{\mathrm{int}}=\frac{2e}{mc}\sum_{n=1}^{\mathrm{occ}}\langle\phi_n(t)|\mathbf{p}\cdot\mathbf{A}(t)|\phi_n(t)\rangle+\frac{L^3}{c}(\dot{\mathbf{A}}\cdot\mathbf{P}+\mathbf{A}\cdot\dot{\mathbf{P}}). \tag{13}$$

The first term can be related to the expectation value of the current **J** flowing through the periodic cell

$$\mathbf{J}=-\frac{2e}{mL^3}\sum_{n=1}^{\mathrm{occ}}\langle\phi_n(t)|\mathbf{p}+\frac{e}{c}\mathbf{A}(\mathbf{r},t)|\phi_n(t)\rangle. \tag{14}$$

Again ignoring terms second order in the vector potential the interaction functional can then be written as

$$E_{\mathrm{int}}=-\frac{L^3}{c}\mathbf{J}\cdot\mathbf{A}+\frac{L^3}{c}(\dot{\mathbf{A}}\cdot\mathbf{P}+\mathbf{A}\cdot\dot{\mathbf{P}}). \tag{15}$$

The key equation leading to the final result is the familiar relation between the time derivative of polarization and the current

$$\dot{\mathbf{P}}=\mathbf{J}. \tag{16}$$

A proof of Eq. (16) for the dipole polarization of Eq. (10) can be found in the Appendix. Inserting together with Eq. (2) we obtain the density functional form of the dipole approximation

$$E_{\mathrm{int}}=-L^3\mathbf{E_T}\cdot\mathbf{P}. \tag{17}$$

B. Dynamical polarization in extended systems

In condensed molecular systems the Clausius–Mossotti approximation is not strictly valid because of the small but finite overlap of molecular charge distributions. However, if the molecular identity is preserved, which can be considered as the definition of a condensed molecular system, it would seem that a "modified" form of the dipole approximation might still apply. Indeed, this is the assumption underlying perturbative treatments of molecular interactions and spectroscopy (see, e.g., Ref. 57). This approach crucially depends on an expansion in a basis of zero order molecular orbitals of individual molecules, which has frustrated the implementation in a plane wave basis set codes, where such a basis is not apriori available. This problem has recently been solved in the framework of the modern theory of polarization developed by Vanderbilt, Resta, and others.[38–43] Their approach enables us to define and compute the polarization in an extended system without any partitioning in molecular units. The central result in this formalism is the Berry phase expression for the electronic polarization **P**, which in the Γ point approximation valid for large supercells can be written as

$$P_\mu=\frac{2e}{G_\mu L^3}\,\mathrm{Im}\ln\det\mathbf{S}, \tag{18}$$

where μ denotes a Cartesian component $\mu=x,y,z$, assuming a cubic cell of length L, and $\mathbf{G}_\mu$ is a vector spanning the corresponding reciprocal lattice with length $G_\mu=2\pi/L$. (For generalization to the lattice of lower symmetry, see Ref. 58.) The matrix **S** is defined by the matrix elements of a phase operator with respect to the Kohn–Sham states ϕ_m (assuming a spin-restricted description)

$$S_{mn}=\langle\phi_m|e^{-i\mathbf{G}_\mu\cdot\mathbf{r}}|\phi_n\rangle. \tag{19}$$

The Berry phase expression for the polarization, and the equivalent formulation in terms of Wannier functions, has initiated a revolution in the electronic structure computation of the condensed phase. In Car–Parrinello simulation, it has opened up the way to "first principle" computation of vibrational spectra of finite temperature condensed molecular systems. This approach was pioneered by Silvestrelli *et al.*[59] in a study of the infrared absorption of liquid water (for a application to an aqueous organic molecule, see Ref. 60) and has also been used in a calculation of Raman spectra of ice.[61]

Equation (18) was derived for ground state systems. The present application to electronic spectroscopy is based on an extension to excited states achieved by replacing the Kohn–Sham (KS) orbitals in Eq. (19) by the time dependent KS orbitals $\phi_n(\mathbf{r},t)$,

$$P_\mu(t)=\frac{2e}{G_\mu L^3}\,\mathrm{Im}\ln\det\langle\phi_m(t)|e^{-i\mathbf{G}_\mu\cdot\mathbf{r}}|\phi_n(t)\rangle. \tag{20}$$

The Berry phase expression Eq. (20) for the dynamical polarization is, at the present, an ansatz, satisfying a number of necessary conditions. One of these conditions, which is absolutely vital, is the relation between the time derivative of the polarization and the current [Eq. (16)]. In the Appendix we will give a demonstration that this equation is still valid. This was the only property of polarization needed in the derivation of the dipole approximation of the previous section, and hence, we conclude that also Eq. (17) still holds when the polarization is replaced by the Berry phase form.

Note, that neither Eq. (20) nor the argument leading to Eq. (17) requires that the system is molecular, which suggests that electronic spectra of covalent solids (semiconductors), as long as they are insulators, can be treated in the same way.

C. Time dependent linear response method

The time dependent Kohn–Sham equation derived according to the Runge–Gross scheme[1] from the total energy functional of Eq. (7) can be written as

$$\left[-\frac{\hbar^2}{2m}\nabla^2+V_{\mathrm{eff}}(\mathbf{r},t)\right]\phi_n(\mathbf{r},t)=\hbar i\frac{\partial}{\partial t}\phi_n(\mathbf{r},t) \tag{21}$$

with local single-particle potential V_{eff} given by

$$V_{\mathrm{eff}}(\mathbf{r},t)=\sum_I V_I(\mathbf{r}-\mathbf{R}_I)+V_{\mathrm{int}}(\mathbf{r},t)+\int \mathrm{d}\mathbf{r}'\frac{n(\mathbf{r}',t)}{|\mathbf{r}-\mathbf{r}'|}+V_{\mathrm{xc}}[n](\mathbf{r},t), \tag{22}$$

where V_I is the potential due to the nuclei [see Eq. (1)]. Just as the exchange correlation potential V_{xc} (in ALDA) is obtained by a functional derivative

$$V_{\mathrm{xc}}(\mathbf{r},t)=\frac{\delta E_{\mathrm{xc}}}{\delta n(\mathbf{r},t)}, \tag{23}$$

so is, in principle, the interaction potential describing the perturbation

$$V_{\mathrm{int}}(\mathbf{r},t)=\frac{\delta E_{\mathrm{int}}}{\delta n(\mathbf{r},t)}=-L^3\mathbf{E}_T\cdot\frac{\delta\mathbf{P}}{\delta n(\mathbf{r},t)}, \tag{24}$$

where we have substituted the dipole approximation Eq. (17). For the dipole form of the polarization [Eq. (10)] evaluation of the functional derivative yields the familiar $e\mathbf{r}$ potential. The way we have handled the Berry phase polarization, for which the functional derivative with respect to density is not explicitly known, will be outlined in Sec. III E.

In linear response theory the coupling to a dynamical probe, such as V_{int} of Eq. (24), is treated as a harmonic perturbation of frequency ω,

$$\delta V(\mathbf{r},t)=\delta V^+(\mathbf{r})e^{i\omega t}+\delta V^-(\mathbf{r})e^{-i\omega t}. \tag{25}$$

The perturbation will induce a change in the effective potential given to first order by

$$\delta V_{\mathrm{eff}}(\mathbf{r},t)=\delta V(\mathbf{r},t)+\delta V_{\mathrm{SCF}}(\mathbf{r},t), \tag{26}$$

where

$$\delta V_{\mathrm{SCF}}(\mathbf{r},\pm\omega)=\int \mathrm{d}\mathbf{r}'\left\{\frac{n^{\{1\}}(\mathbf{r}',\pm\omega)}{|\mathbf{r}-\mathbf{r}'|}+\left.\frac{\delta^2E_{\mathrm{xc}}}{\delta n(\mathbf{r})\,\delta n(\mathbf{r}')}\right|_{n=n^{\{0\}}}n^{\{1\}}(\mathbf{r}',\pm\omega)\right\} \tag{27}$$

is the change in the self-consistent field in the frequency domain. The linear density response

$$n^{\{1\}}(\mathbf{r},\pm\omega)=2\sum_{i=1}^{\mathrm{occ}}\langle\phi_i^{\{\mp\}}|\mathbf{r}\rangle\langle\mathbf{r}|\phi_i^{\{0\}}\rangle+\langle\phi_i^{\{0\}}|\mathbf{r}\rangle\langle\mathbf{r}|\phi_i^{\{\pm\}}\rangle \tag{28}$$

is expressed in terms of a set of linear response orbitals $\{\phi_i^{\{\pm\}}\}$ which can be chosen to be orthogonal to the subspace of the ground state orbitals:

$$\langle\phi_i^{\{\pm\}}|\phi_j^{\{0\}}\rangle=0. \tag{29}$$

This leads to a set of coupled perturbed Kohn–Sham equations[11]

$$\sum_{j=1}^{\mathrm{occ}}(\epsilon_{ij}-(F\pm\omega)\delta_{ij})|\phi_j^{\{\pm\}}\rangle=Q(\delta V^{\{\pm\}}+\delta V_{\mathrm{SCF}}(\pm\omega))|\phi_i^{\{0\}}\rangle, \tag{30}$$

where

$$Q=\mathbf{1}-\sum_{k=1}^{\mathrm{occ}}|\phi_k^{\{0\}}\rangle\langle\phi_k^{\{0\}}| \tag{31}$$

is the projector on the subspace of the unperturbed unoccupied states, F is the Kohn–Sham Hamiltonian and ϵ_{ij} are the set of Lagrange multipliers ensuring the orthonormality of ground state orbitals. Excitation energies correspond to the poles of the response functions[3] and lead to singularity in Eq. (30). Thus they are solutions to the equations

$$\sum_{j=1}^{\mathrm{occ}}(F\delta_{ij}-\epsilon_{ij})|\phi_j^{\{\pm\}}\rangle+Q\,\delta V_{\mathrm{SCF}}(\pm\omega)|\phi_i^{\{0\}}\rangle=\mp\omega|\phi_i^{\{\pm\}}\rangle. \tag{32}$$

D. Excitation energies in Tamm-Dancoff approximation

The solution of Eq. (32) can be cast as a non-Hermitian eigenvalue equation with eigenvalues ω^2.[3,11] In the Tamm–Dancoff approximation (TDA) (Refs. 62–64) this can be simplified to a Hermitian problem with excitation energies as eigenvalues. By expanding the ground-state Kohn–Sham orbitals $\{\phi_i^{\{0\}}\}$ and linear response orbitals $\{\phi_i^{\{\pm\}}\}$ in the orthogonal basis set functions $\pi_p(\mathbf{r})$ (which will be assumed here to be plane waves, $\pi_p=L^{-3/2}e^{i\mathbf{G}\cdot\mathbf{r}}$, with $\mathbf{G}$ a reciprocal lattice vector of the simulation supercell)

$$\phi_i^{\{0\}}(\mathbf{r})=\sum_{p=1}^{M}c_{pi}^{\{0\}}\pi_p(\mathbf{r}), \tag{33}$$

$$\phi_i^{\{\pm\}}(\mathbf{r})=\sum_{p=1}^{M}c_{pi}^{\{\pm\}}\pi_p(\mathbf{r}), \tag{34}$$

and introducing new sets of coefficients

$$x_{pi}=(c_{pi}^{\{+\}}+c_{pi}^{\{-\}}),\qquad y_{pi}=(c_{pi}^{\{+\}}-c_{pi}^{\{-\}}), \tag{35}$$

Eq. (30) can be recast as

$$(\mathcal{A}+\mathcal{B})\mathbf{x}^\mu+\omega\mathbf{y}^\mu=\mathbf{b}^\mu,\qquad(\mathcal{A}-\mathcal{B})\mathbf{y}^\mu+\omega\mathbf{x}^\mu=\mathbf{0}, \tag{36}$$

where the superscript μ indicates the direction of the induced polarization. The operators $\mathcal{A}$ and $\mathcal{B}$ act on a general ($M\times N$) matrix $\mathbf{z}$ according to

$$\mathcal{A}\mathbf{z}=(\mathbf{F}\mathbf{z}-\mathbf{z}\boldsymbol{\epsilon})+\mathbf{Q}\mathbf{W}\mathbf{c},\quad \mathcal{B}\mathbf{z}=\mathbf{Q}\mathbf{W}\mathbf{c}, \tag{37}$$

where the Kohn–Sham Hamiltonian,

$$F_{pq}=\langle \pi_p|F|\pi_q\rangle, \tag{38}$$

Lagrange multiplier,

$$\epsilon_{ij}=\sum_{pq}\ (c_{pi}^{\{0\}})^{\star}F_{pq}c_{qj}^{\{0\}}, \tag{39}$$

virtual state projector,

$$Q_{pq}=\delta_{pq}-\sum_{i=1}^{\mathrm{occ}}\ c_{pi}^{\{0\}}(c_{qi}^{\{0\}})^{\star}, \tag{40}$$

and δV_{SCF},

$$W_{pq}=\langle \pi_p|\,\delta V_{\mathrm{SCF}}|\pi_q\rangle, \tag{41}$$

matrix elements are all expressed in the plane-wave representation. The matrix

$$\mathbf{b}^{\mu}=2\mathbf{Q}\mathbf{f}^{\mu}\mathbf{c}, \tag{42}$$

includes the $(M\times M)$ perturbation matrix $\mathbf{f}$, whose elements are given by

$$f_{pq}^{\mu}=-L^3\langle \pi_p|\left.\frac{\delta P_{\mu}}{\delta n(\mathbf{r})}\right|_{n=n^{(0)}}|\pi_q\rangle. \tag{43}$$

Within the present formalism, the TDA amounts to setting the expansion coefficients $c_{pi}^{\{+\}}$ to zero in Eq. (34), leading to $\mathbf{x}^{\mu}=-\mathbf{y}^{\mu}$. Equation (36) is therefore replaced by

$$(\mathcal{A}-\omega\mathbf{1})\mathbf{x}^{\mu}=\mathbf{b}^{\mu}. \tag{44}$$

The excitation energies are now computed from the Hermitian eigenvalue problem

$$\mathcal{A}\mathbf{x}_I=\omega_I\mathbf{x}_I. \tag{45}$$

Provided the eigenvectors $\mathbf{x}_I$ are normalized the linear response can then be obtained using the spectral resolution of $\mathcal{A}$,

$$\mathbf{x}^{\mu}=\frac{\mathbf{b}^{\mu}}{\mathcal{A}-\omega\mathbf{1}}=\sum_I\ \frac{\mathbf{x}_I\mathbf{x}_I^T\mathbf{b}^{\mu}}{\omega_I-\omega}. \tag{46}$$

E. Dynamical polarizability and oscillator strengths

The Berry phase polarization of Eq. (20) is not available as an explicit functional of density. In this respect it resembles exchange correlation functionals containing an exact exchange contribution, such as B3LYP. The common procedure to deal with orbital dependent density functionals in quantum chemistry calculations, is using the orbital derivative rather than the density derivative. This approach, deviating from the true spirit of the Kohn–Sham method, will also be employed here for polarization. In the context of a perturbation calculation this amounts to replacing the factor $\mathbf{fc}$ in the expression Eq. (42) for the driving force $\mathbf{b}$ by the $M\times N$ matrix $\mathbf{d}$ defined as[65]

$$d_{pi}^{\mu}=-L^3\int\ d\mathbf{r}\ \pi_p^{*}(\mathbf{r})\left.\frac{\delta P_{\mu}[\boldsymbol{\phi}]}{\delta\phi_i^{*}(\mathbf{r})}\right|_{\phi_i=\phi_i^{\{0\}}}. \tag{47}$$

The key to compute this functional derivative is the expression for the first order variation of the Berry phase (see, e.g., Ref. 65)

$$\delta P_{\mu}=-\sum_{\nu}\ \frac{2e}{L^3|\mathbf{G}_{\mu}|}\,\mathrm{Im}\ \left\{\sum_{ij}^{\mathrm{occ}}\ [\langle \delta\phi_i^{\{\nu\}}|e^{-i\mathbf{G}_{\mu}\cdot\mathbf{r}}|\phi_j^{\{0\}}\rangle + \langle \phi_i^{\{0\}}|e^{-i\mathbf{G}_{\mu}\cdot\mathbf{r}}|\phi_j^{\{\nu\}}\rangle][\langle \phi_j^{\{0\}}|e^{-i\mathbf{G}_{\nu}\cdot\mathbf{r}}|\phi_i^{\{0\}}\rangle]^{-1}\right\}, \tag{48}$$

where $\phi_i^{\{\nu\}}\equiv\phi_i^{\{\nu\}}(t)$ represents the linear response of $\phi_i^{\{0\}}$ to a small perturbation $E_{\nu}(t)$ in the Cartesian direction ν. Equation (48) can be applied immediately to obtain the polarizability. In the vector notation introduced above this reads

$$\alpha_{\mu\nu}(\omega)=\frac{2}{|\mathbf{G}_{\mu}|}\,\mathrm{Im}[(\mathbf{x}^{\nu})^T\mathbf{g}^{\mu}\mathbf{c}+\mathbf{c}^T\mathbf{g}^{\mu}\mathbf{x}^{\nu}][(\mathbf{c}^T\mathbf{g}^{\nu}\mathbf{c})^{-1}]^T, \tag{49}$$

where we have defined

$$g_{pq}^{\mu}=\langle \pi_p|e^{-i\mathbf{G}_{\mu}\cdot\mathbf{r}}|\pi_q\rangle. \tag{50}$$

Inserting the TDA solution of Eq. (46) for the first order orbitals, we can rewrite Eq. (49) as

$$\alpha_{\mu\nu}(\omega)=\frac{4}{|\mathbf{G}_{\mu}|}\,\mathrm{Im}[(\mathbf{b}^{\mu})^T\mathbf{x}(\mathcal{A}-\omega\mathbf{1})^{-1}\mathbf{x}^T\mathbf{g}^{\nu}\mathbf{c}]\times[(\mathbf{c}^T\mathbf{g}^{\nu}\mathbf{c})^{-1}]^T \tag{51}$$

and obtain for the oscillator strength of mode I, following standard time dependent linear response theory

$$f_I=-\frac{4}{3}\,\omega_I\sum_{\mu}\ \frac{1}{|\mathbf{G}_{\mu}|}\,\mathrm{Im}[(\mathbf{b}^{\mu})^T\mathbf{x}_I(\mathbf{x}_I)^T\mathbf{g}^{\mu}\mathbf{c}][(\mathbf{c}^T\mathbf{g}^{\mu}\mathbf{c})^{-1}]^T. \tag{52}$$

For $\mathbf{b}$ we must use the generalization of Eq. (42) with $\mathbf{d}$ of Eq. (47) instead of the product $\mathbf{fc}$,

$$\mathbf{b}^{\mu}=\mathbf{Q}\mathbf{d}^{\mu}=2\ \ [\mathbf{d}^{\mu}-\mathbf{c}\ \ (\mathbf{c}^T\mathbf{d}^{\mu})]. \tag{53}$$

The second equality follows as a consequence of Eq. (40). Substituted into Eq. (52) this leads after some rearrangement [note $\mathbf{c}^T\mathbf{x}=\mathbf{0}$, as the linear response orbitals are orthogonal to the ground-state orbitals, Eq. (29)] to

$$f_I=-\frac{8}{3}\,\omega_I\sum_{\mu}\ \frac{1}{|\mathbf{G}_{\mu}|}\,\mathrm{Im}((\mathbf{d}^{\mu})^T\mathbf{x}_I)(\mathbf{x}_I^T\mathbf{g}^{\mu}\mathbf{c})[(\mathbf{c}^T\mathbf{g}^{\mu}\mathbf{c})^{-1}]^T. \tag{54}$$

The complex arithmetic in Eq. (54) is somewhat cumbersome. From a practical point of view its function is to ensure that the transition dipoles satisfy the Born–von Karman periodic boundary conditions as assumed when the Γ point approximation is enforced. With this in mind, we can simplify Eq. (54), while strictly adhering to periodic boundary conditions, by setting

$$\mathbf{d}^{\mu}\approx\frac{\mathbf{g}^{\mu}\mathbf{c}}{|\mathbf{G}_{\mu}|}. \tag{55}$$

Introducing the periodic transition dipoles

$$(\gamma_{01}^{\mu})_{ij} = i \frac{\langle \phi_i^{\{0\}} | e^{-i\mathbf{G}_\mu \cdot \mathbf{r}} | \phi_j^{\{-\}} \rangle}{|\mathbf{G}_\mu|}, \tag{56}$$

$$(\gamma_{10}^{\mu})_{ij} = i \frac{\langle \phi_i^{\{-\}} | e^{-i\mathbf{G}_\mu \cdot \mathbf{r}} | \phi_j^{\{0\}} \rangle}{|\mathbf{G}_\mu|}, \tag{57}$$

and

$$(\gamma_{00}^{\mu})_{ij} = i \frac{\langle \phi_i^{\{0\}} | e^{-i\mathbf{G}_\mu \cdot \mathbf{r}} | \phi_j^{\{0\}} \rangle}{|\mathbf{G}_\mu|}. \tag{58}$$

the oscillator strength can be expressed as

$$f_I = -\frac{8}{3}\omega_I \sum_{\mu} \frac{1}{|\mathbf{G}_\mu|^2} \mathrm{Im}\, \gamma_{01}^{\mu} \gamma_{10}^{\mu} [(\gamma_{00}^{\mu})^{-1}]^T. \tag{59}$$

We note that, in the limit of large cell size and for localized states, $\gamma_{00}^{\mu}|\mathbf{G}_\mu| \to \mathbf{1}i$, and an expansion of the exponential function in Eq. (57) leads to the conventional formula for the oscillator strengths in confined systems,

$$f_I = \tfrac{2}{3}\omega_I \sum_{\mu} |\boldsymbol{P}_{01}^{\mu}|^2, \tag{60}$$

where $\boldsymbol{P}_{01}^{\mu} = \langle \Psi_0 | x_\mu | \Psi_1 \rangle$ is the "transition dipole" for an excitation from the ground-state Ψ_0 to an excited state Ψ_1, whose energies differ by $\omega_I = E_1 - E_0$.

F. Analysis of the excitations

The eigenvectors $\mathbf{x}_I$ can be used to compute the relative contribution of Kohn–Sham single-particle excitations to the electronic transition I. To this end a set of L virtual orbitals $\{\psi_i\}$, in canonical form, need be computed from the ground-state Kohn–Sham potential, expressed in plane-wave expansion by

$$|\psi_i\rangle = \sum_{p=1}^{M} v_{pi} \pi_p. \tag{61}$$

The set of virtual orbitals is supposed to be large enough to allow a complete expansion of the linear response orbitals associated with the transition I,

$$|\phi^{\{-\}}\rangle = \sum_{j=1}^{L} w_{i\to j} \psi_j. \tag{62}$$

The "weight" of the transition from the occupied Kohn-Sham orbital i to the virtual orbital j for the excitation I, $w_{i\to j}$, is given by

$$w_{i\to j} = \langle \psi_j | \phi^{\{-\}} \rangle = \sum_{p=1}^{M} v_{pj}^{\star} x_{pi}. \tag{63}$$

An important additional piece of information obtained in a Car–Parrinello MD simulation is the modulation by thermal motion of the ions. The frequency ω_I and oscillator strength f_I of a transition I follow the adiabatic motion of the molecules, producing a time series $\omega_I(t)$ respectively $f_I(t)$. The single transition line I is broadened into a band with a spectral profile $F_I(\omega)$ which can be expressed as

$$F_I(\omega) = \frac{1}{T}\int_T \mathrm{d}t f_I(t)\, \delta(\omega_I(t) - \omega) = \frac{1}{N_R}\sum_{R=1}^{N_R} f_I^R \delta(\omega_I^R - \omega), \tag{64}$$

where T is the duration of the MD run. The second identity gives the discretized estimator used to compute $F_I(\omega)$. It has the form of an average over N_R sample configurations R. The line shape $F_I(\omega)$ should be distinguished from the the normalized excitation energy density of states (EEDOS) defined as

$$\mathrm{EEDOS}_I(\omega) = \frac{1}{T}\int_T \mathrm{d}t\, \delta(\omega_I(t) - \omega) = \frac{1}{N_R}\sum_{R=1}^{N_R} \delta(\omega_I^R - \omega), \tag{65}$$

describing the distribution of frequencies ω_I without the weights of the intensities. The overall intensity of a band can be quantified by the *time averaged* oscillator strength of a mode I,

$$f_I = \frac{1}{T}\int_T \mathrm{d}t\, f_I(t) = \frac{1}{N_R}\sum_{R=1}^{N_R} f_I^R. \tag{66}$$

IV. DETAILS OF CALCULATIONS

Kohn–Sham density functional theory calculations and *ab initio* molecular dynamics (MD) simulations were performed using CPMD.[66] All the systems were treated within periodic boundary conditions and the Kohn–Sham eigenvectors were expanded in plane-waves at the Γ point of the Brillouin zone up to a kinetic energy cutoff of 70 Ry. For the gas-phase systems [$(CH_3)_2CO$ and $(CH_3)_2CO\cdot(H_2O)_2$], ion–electron interactions were described using *ab initio* norm-conserving dual-space pseudopotentials,[67] with separate potentials for s and p components for C and O, and a local potential for H. For the acetone–water solution, we used pseudopotentials of the Troullier–Martins-type[68] with analogous nonlocal projectors. All the pseudopotentials had been tested extensively in previous calculations. MD simulations were performed within the Car–Parrinello scheme,[12] with exchange-correlation energy described at the BLYP (Refs. 69, 70) level of theory. A fictitious mass of 600 a.u. and an integration time step of 5 a.u. were used. Temperature was controlled through a Nosé–Hoover thermostat. Excitation energies were computed from TDA TDDFT (Refs. 63, 64) within the local density approximation to the exchange-correlation kernel.[4] Equation (45) was solved using Davidson's iterative subspace method.[9,71,72]

V. RESULTS AND DISCUSSION

A. Acetone molecule

As a preliminary test case, the $n \to \pi^*$ transition energy in gas-phase acetone was computed. The molecular system was studied using a periodically repeated simulation supercell of size $a = 15.88$ Å. The geometry was optimized at the

BLYP level, and the 10 lowest excitation energies were estimated starting from the Kohn–Sham eigenvectors and ground-state density. According to the assignment scheme described in Sec. III F the lowest-energy excitation corresponds to a pure HOMO→LUMO (Kohn–Sham $n\rightarrow\pi^*$) transition, with a transition energy $\omega_{\mathrm{TDDFT}}=4.18$ eV. This should be compared to the *time independent* Kohn–Sham estimate $\omega_{\mathrm{KS}}\equiv\epsilon_{\mathrm{LUMO}}-\epsilon_{\mathrm{HOMO}}=3.91$ eV and to the available experimental values, $\omega_{\mathrm{exp}}=4.3-4.5$ eV (Refs. 45, 49, 73, 74, 75) (see also Table I). Overall, the application of the TDDFT procedure brings about a shift of the transition energy of ~ 0.27 eV with respect to the time independent Kohn–Sham value (an increase of $\sim 7\%$ of the Kohn–Sham HOMO-LUMO gap), but it does not induce admixture of orbital character from lower- (occupied) or higher- (virtual) states. It remains an open question whether better agreement with experiment can be accomplished by solving the non-Hermitian problem of Eq. (36) without applying the TDA, although in general the corrections in a full TDDFT scheme seem to be minimal.[63,64] Further improvement may require a more sophisticated representations of the exchange-correlation potential in the ground-state calculation and of the kernel in the TDDFT procedure, e.g., through inclusion of exact (Hartree–Fock) exchange.[8]

The oscillator strength, estimated through Eq. (59), turned out to be lower than 3×10^{-5}, consistent with the symmetry-forbidden character of the transition. The small nonzero value may be explained by slight deviations from perfect C_2 symmetry introduced by the (unconstrained) geometry optimization procedure, or by spurious interactions between molecules in neighboring cells. In order to ascertain the importance of thermal relaxation effects on the transition intensity, we performed a Car–Parrinello MD simulation at 298 K. We computed the time averaged oscillator strength f_I of Eq. (66) for the $n\rightarrow\pi^*$ transition by averaging over $N_R=100$ instantaneous ionic configurations, sampled from a run spanning an overall time of $T=2.4$ ps. The result is $f_{n\rightarrow\pi^*}=2\times10^{-4}$, which is comparable to the experimental estimate $f_{n\rightarrow\pi^*}\simeq4\times10^{-4}$.[49,76] We also estimated the full width at half maximum (FWHM) of the inhomogeneous line shape $F_{n\rightarrow\pi^*}(\omega)$ as defined in Eq. (64). Our value of ~ 0.6 eV is smaller than the experimental value (0.86 eV), which may arguably be attributed to the expected systematic underestimation of the oscillator strengths within the Tamm–Dancoff approximation[63,64] or neglect of quantum effects. Overall, these results are nonetheless indicative of the degree of accuracy which our approach is able to yield when applied to finite-size molecular systems.

B. Gas-phase $(CH_3)_2CO\cdot(H_2O)_2$

High-level quantum-chemical calculations have frequently been used to characterize stability, equilibrium geometry, and other static properties of molecules surrounded by a small number of solvent molecules, as clusters in the gas phase, and to estimate transition energies of selected electronic excitations.[53,77–79] In acetone–water clusters (containing up to 3 water molecules), the $n\rightarrow\pi^*$ transition energy was found to blueshift of 0.05–0.40 eV upon water coordination, depending on the number of water molecules and cluster geometry. Oscillator strengths increase up to $\sim10^{-4}$.[53] This approach is applied here to $(CH_3)_2CO\cdot(H_2O)_2$. The gas-phase cluster was modeled using a cubic super-cell of size $a=15.88$ Å. The geometry was carefully optimized starting from the 0 K structure of acetone, with two water molecules roughly orienting one of their O–H bonds toward the carbonyl oxygen, at a distance of approximately 2 Å. We performed a short (1.2 ps) Car–Parrinello MD simulation at 25 K, followed by simulated annealing, until the forces on the ions were lower than $\sim1\times10^{-3}$ a.u. A full geometry optimization was then performed leading to a configuration with all ionic forces lower than 5×10^{-4} a.u. (Fig. 1). In this geometry the water molecules, the carbonyl group, and the methyl carbon atom are rather close to lying in the same plane, despite the fact that the initial geometry was not constrained to be planar.

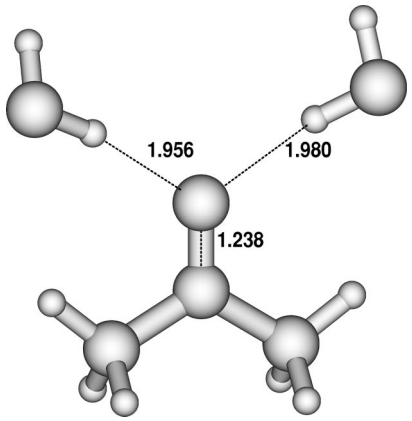

FIG. 1. Optimized geometry of gas-phase $(CH_3)_2CO\cdot(H_2O)_2$. Selected distances (Å) are indicated.

The Kohn–Sham eigenvalue energies of the complex are shown in Fig. 2, where they are also compared to the orbital energies of isolated water and acetone in the gas phase. The alignment of the $1b_1$ (HOMO) orbitals of the two water molecules which are both in-plane with the carbonyl bond, and the relative proximity in energy to the n orbital of acetone results in the concurrence of three Kohn–Sham states at the Fermi energy within an interval $E_{\mathrm{HOMO}}-E_{\mathrm{HOMO\text{-}2}}=0.16$ eV. These states delocalize over the whole cluster (Fig. 2, right panel). Two of them (HOMO and HOMO-1) are nearly degenerate ($\epsilon_{\mathrm{HOMO}}-\epsilon_{\mathrm{HOMO\text{-}1}}=0.04$) eV, and the third is at slightly lower energy. The LUMO in the complex maintains pure acetone π^* character, and remains well separated from higher-energy empty orbitals. This result confirms that the π^* orbital is not affected by direct chemical interaction with the water molecules and its (modest) stabilization in solution may therefore arise solely from electrostatic interaction with the solvent.

The HOMO→π^* and HOMO-1→π^* Kohn–Sham transition energies are only slightly larger than the Kohn–Sham $n\rightarrow\pi^*$ transition energy in acetone (Table I), while the HOMO-2→π^* is 0.20 eV higher in energy. TDDFT excitation energies for the two lowest-energy transitions change only modestly ($\Delta\omega=+0.01$ eV) with respect to the Kohn–Sham estimates. The third transition energy (the highest of

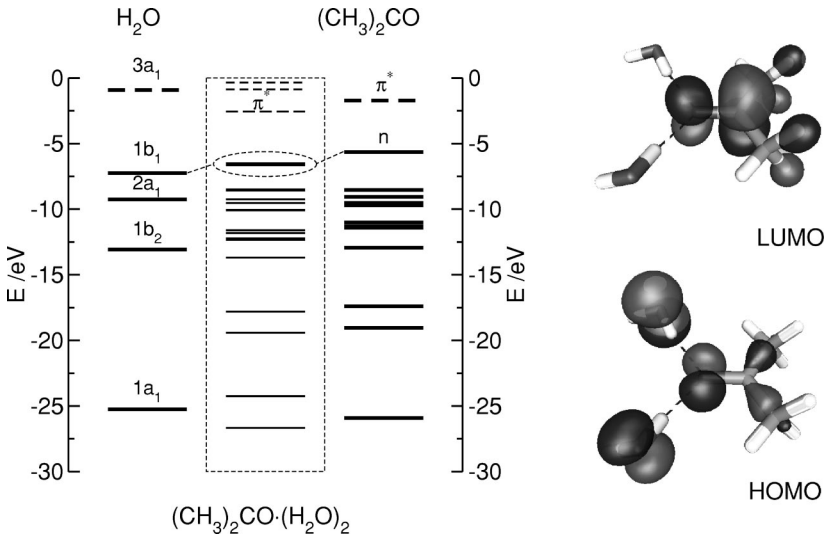

FIG. 2. (Left panel) Kohn–Sham eigenvalues for gas-phase $(CH_3)_2CO\cdot(H_2O)_2$, H_2O, and $(CH_3)_2CO$. Virtual states are indicated by dashed lines. (Right panel) Frontier orbitals of $(CH_3)_2CO\cdot(H_2O)_2$.

the transitions from the three state n manifold) is however significantly increased (Fig. 3), $\Delta\omega=0.25$ eV, which parallels the $n\rightarrow\pi^*$ energy shift in acetone (0.27 eV). The corresponding excitation energy is $\sim$0.16 eV higher compared to acetone (Fig. 3).

The effects of thermal relaxation on the transition energies were studied at 25 K. This low temperature was necessary to prevent dissociation into molecular fragments during the simulation (this appeared to occur, on the few picosecond scale, already at 50 K). 1 ps of thermal equilibration was allowed, followed by a production run of $\sim$2.7 ps. The calculation of the TDDFT excitation energies was performed, again, on 100 instantaneous ion configurations, equally spaced in time to cover a period of 2.4 ps. The 10 lowest excitations were computed at each configuration, in order to assess whether higher energy transitions may occasionally mix with the three lowest ones of interest. As for gas-phase acetone, this was found never to occur.

We show in Fig. 4 the normalized excitation energy density of states (EEDOS, lower panel) as defined in Eq. (65). The full (transition resolved) electronic excitation spectrum $F_I(\omega)$ is given in the upper panel. The two lowest transitions (ω_1 and ω_2) give rise to broad (FWHM$\simeq$0.2) features, frequently overlapping with each other, whereas a well separated sharper band appears at slightly higher energy. Intensity-weighted mean transition energies, $\bar{\omega}_I=\int d\omega\, F_I(\omega)\omega$, and frequency-integrated intensities, Eq. (66), are reported in Table I. The thermal motion leaves $\bar{\omega}_1$ and $\bar{\omega}_3$ virtually unchanged with respect to the values of the optimised (zero temperature) geometry, while $\bar{\omega}_2$ is shifted to higher energies by $\sim$0.09 eV. The integrated f_1 and f_2 oscillator strengths decrease slightly, whereas f_3 is unvaried. Note also that the third (highest) frequency transition is about an order of magnitude weaker in intensity compared to the lower two transitions (Table I).

The contrasting behavior of the $\omega_1-\omega_2$ and the ω_3 bands is suggestive of a different nature of the underlying excitation processes. All three Kohn–Sham orbitals close to the Fermi energy have mixed water–acetone character. In spite of this similarity we interpret the differences in the transitions to the π^* state as arising from a varying degree of intermolecular (water$\rightarrow$acetone) charge-transfer character. The ω_3 excitation, in this picture, has predominant, but not exclusive, $n\rightarrow\pi^*$ character, whereas the two low frequency transitions mainly consist of solvent$\rightarrow$solute charge transfers. This assignment is in line with the established poor

TABLE I. Time-averaged electronic excitation energies (eV) from Kohn–Sham eigenvalue energy differences ($\bar{\omega}^{KS}$) and from TDDFT ($\bar{\omega}^{TDDFT}$). f are TDDFT transition intensities, estimated through Eq. (66). Experimental transition energies (ω^{exp}) and intensities (f^{exp}) for acetone in the gas phase (Refs. 49, 73, 45, 74, 75) and in solution (Refs. 49–52) are reported for comparison. The values quoted in brackets for $(CH_3)_2CO\cdot(H_2O)_2$ ($T=0$ K) are CIS and CASSCF estimates of Liao *et al.* (Ref. 53) for a gas-phase cluster of analogous composition though differing in geometry from our optimized structure.

System	Transition	$\bar{\omega}^{KS}$	$\bar{\omega}^{TDDFT}$	ω^{exp}	f	f^{exp}
$(CH_3)_2CO$ ($T=298$ K)						
	$n\rightarrow\pi^*$	3.91	4.18	4.3–4.5	1.8×10^{-4}	4×10^{-4}
$(CH_3)_2CO\cdot(H_2O)_2$ ($T=0$ K)						
	HOMO$\rightarrow\pi^*$	3.95	3.97		1.1×10^{-3}	
	HOMO-1$\rightarrow\pi^*$	3.99	4.01		1.0×10^{-3}	
	HOMO-2$\rightarrow\pi^*$	4.11	4.35	[4.75–5.52]	0.7×10^{-4}	[0.1–1.0$\times10^{-5}$]
$(CH_3)_2CO\cdot(H_2O)_2$ ($T=25$ K)						
	HOMO$\rightarrow\pi^*$	3.99	4.01		0.8×10^{-3}	
	HOMO-1$\rightarrow\pi^*$	4.07	4.10		0.7×10^{-3}	
	HOMO-2$\rightarrow\pi^*$	4.18	4.35		0.7×10^{-4}	
$(CH_3)_2CO$ (aq, $T=298$ K)						
	$n\rightarrow\pi^*$		4.37	4.5–4.7	$\sim3\times10^{-4}$	$\sim1\times10^{-3}$

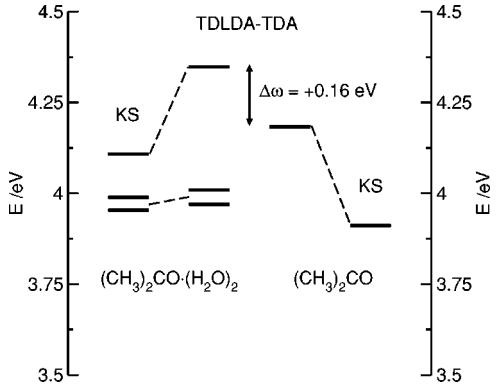

FIG. 3. Kohn–Sham eigenvalue energy differences (KS) and TDDFT transition energies in $(CH_3)_2CO\cdot(H_2O)_2$ and $(CH_3)_2CO$. $\Delta\omega$ is the energy blueshift brought about by water coordination. The two low frequency transitions, which in the TDDFT treatment remain at virtually the uncoupled KS value, are ascribed to solvent→solute charge transfers (see Sec. V B).

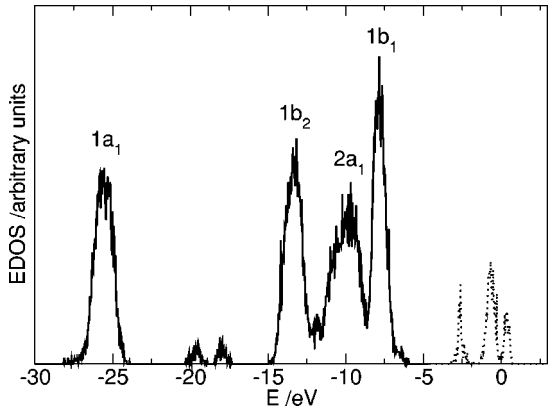

FIG. 5. Finite temperature ($T=298$ K) Kohn–Sham EDOS of $(CH_3)_2CO$ in water. Bands are labeled according to the standard nomenclature for the molecular orbitals of water, unlabeled peaks correspond to acetone states. Dashed lines indicate empty states.

performance of TDDFT in describing charge-transfer excitations.[22–24] Transition energies are badly underestimated with respect to high-level *ab initio* results. The implication for our calculation is that the $\omega_1-\omega_2$ band, assuming the origin of the excited electron to be the nonbonding orbital of water, is strongly redshifted. The correct location should be at much higher frequency with respect to the ω_3 transition. This model could also explain the modest blueshift of the latter transition, $\Delta\omega_3=\omega_3^{(CH_3)_2CO\cdot(H_2O)_2}-\omega_3^{(CH_3)_2CO}=0.17$ eV compared to the CASSCF result of Ref. 53. For the optimized geometry of the $(CH_3)_2CO\cdot(H_2O)_2$ cluster bearing closest resemblance to the system studied here (i.e., with both water molecules hydrogen bonded to the carbonyl oxygen) the CASSCF estimate is $\Delta\omega_{n\to\pi^*}=0.40$ eV. The lower TDDFT result is consistent with a residual charge transfer component in this transition which should be largely of $n\to\pi^*$ character with some admixture of higher acetone excitations. Further support for our interpretation is provided by the difference in intensities. Unlike the n orbital of acetone which is perpendicular to the π^* orbital, the parallel alignment of the $1b_1$ orbitals of the water molecules with the carbonyl π^* maximizes the transition dipole moments.

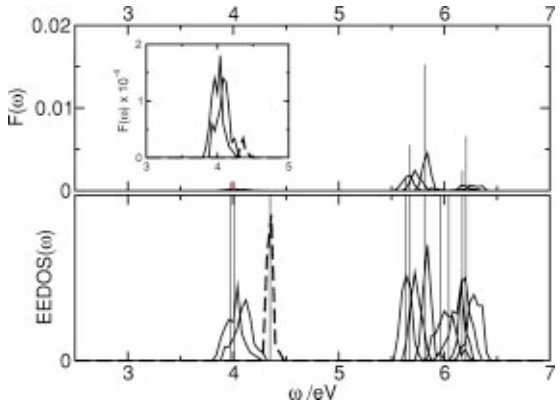

FIG. 4. EEDOS(ω) [in arbitrary units, Eq. (65), lower panel] and (dimensionless) excitation spectrum $F(\omega)$ [Eq. (64) of $(CH_3)_2CO\cdot(H_2O)_2$] at $T=25$ K. Thin vertical lines correspond to transition energies in the optimized geometry. The inset shows details of the bands corresponding to the three lowest excitations. The dashed line indicates the transition with predominant $n\to\pi^*$ character.

C. Acetone water solution

Hydrated acetone was modeled using a periodically repeated cubic simulation supercell of side $a=9.86$ Å, containing one acetone and 28 water molecules. The cell size and the number of water molecules were determined by imposing that the mixed acetone–water system yield a total pressure equal to a sample of liquid water at normal conditions, as computed using classical interaction force-field parameters.[80] A classical MD simulation (65 ps, 298 K) was also used to set up an initial input configuration for a Car–Parrinello MD at the same temperature. A short equilibration time of ~0.4 ps was allowed, followed by a 3 ps production run.

A first shell of hydrogen atoms around the carbonyl oxygen was found at ~2 Å a distance which is only slightly larger than the O(acetone)–H(water) separation in the gas-phase $(CH_3)_2CO\cdot(H_2O)_2$ complex. Examining the details of the dynamical trajectory we observed that although 2 water molecules appeared to be associated with acetone in typical situations, occasionally only one molecule was found to be within the reach of typical hydrogen-bond interactions (~2 Å). In addition, a rapid interchange of the water molecules involved in direct bonding to the carbonyl oxygen was observed, together with wide oscillations (~1 Å) of the O(acetone)–H distance of solvent molecules temporarily bound to acetone.

The finite-temperature Kohn–Sham electron density of states (EDOS), computed from 85 ion configurations spanning 2 ps is plotted in Fig. 5. Some of the bands can easily be interpreted in terms of water molecular orbitals, as indicated by the conventional symmetry labels, other bands (not labeled in the figure) arise from acetone states. The top-energy band ($1b_1$) does however show a tail of states extending at higher energy up to ~−6.0 eV, which raises the Fermi energy with respect to clean liquid water. The origin of this feature is ascribed to one Kohn–Sham state oscillating

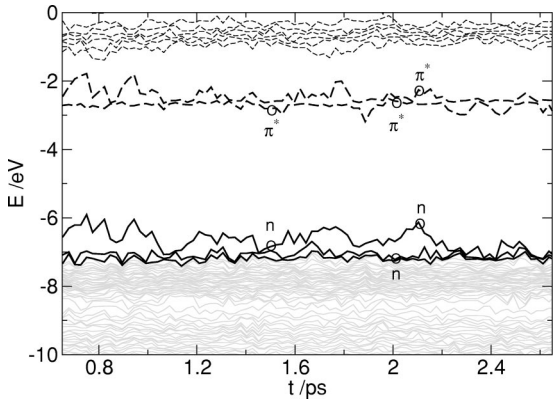

FIG. 6. Variation with time of the one-electron (Kohn–Sham) eigenvalue energies in the model aqueous acetone solution. HOMO, HOMO-1, and HOMO-2 have been distinguished from low-lying states. Dashed lines indicate empty states, with LUMO and LUMO+1 highlighted by thick dashed curves. Circles indicate the energy of the n and π^* orbitals of a few instantaneous atomic configurations discussed in the text.

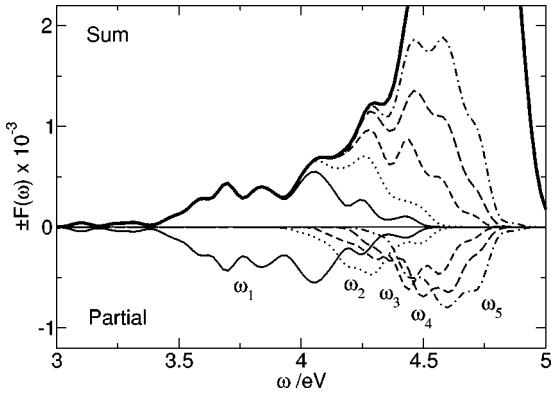

FIG. 8. Electronic absorption spectrum of $(CH_3)_2CO$ in water (upper panel, thick line) and resolution in partial spectra $F_I(\omega)$ [Eq. (64)] corresponding to the lowest five transitions ω_I, $I=1,5$. The lower panel shows the negative of the single-excitation spectra, the thin curves in the upper panel give the corresponding accumulative spectra.

within 1 eV above the top of the $1b_1$ band of water (Fig. 6), with which it can occasionally become degenerate. Frequently, though not always, this quasi-gap state (HOMO) corresponds to the acetone n orbital, for example in the instantaneous configurations marked at $t=1.5$ and $t=2.1$ ps in Fig. 6 (for a graphical representation of the orbitals at $t=1.5$ ps, see Fig. 7). In other situations, e.g., at $t\simeq 2$ ps, the n orbital is buried within the water valence band, corresponding to either HOMO-1 or HOMO-2, and the HOMO of the overall system is replaced by a more delocalized water state. In either case, the n orbital *never* hybridizes with water molecules other than in negligible amounts, at variance with what was observed in gas-phase $(CH_3)_2CO\cdot(H_2O)_2$. This is likely to be related to the more disordered environment surrounding the solute, which lifts the near degeneracy observed for the optimized cluster (Fig. 2) and prevents optimal orbital phase matching from occurring (see Ref. 81 for a more detailed analysis of the interplay between thermal disorder and electronic interactions in liquid water).

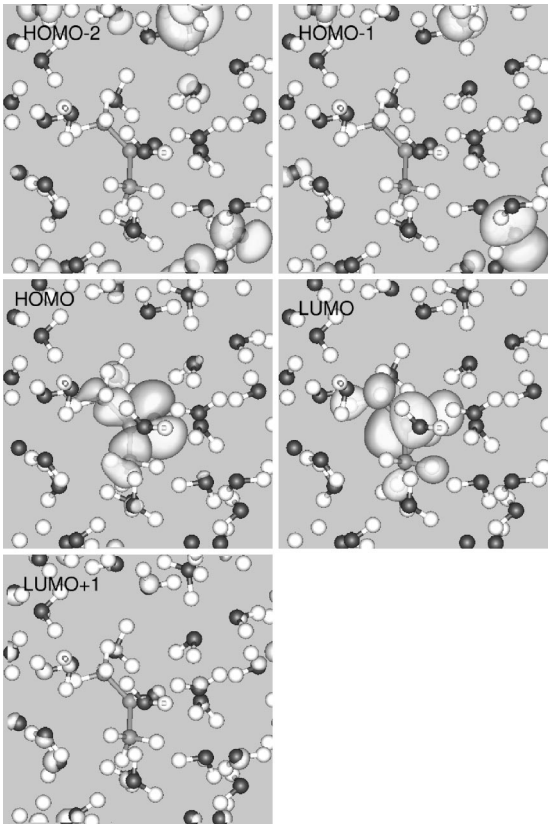

FIG. 7. Selected Kohn–Sham orbitals for the instantaneous atomic configuration at $t=1.5$ ps in Fig. 6. Note that the HOMO and LUMO are localized on the solute at the center.

The empty states lowest in energy (Fig. 6) exhibit a similar alternation between solute and solvent character. One of this pair of nearly degenerate orbitals is almost entirely localized on the solute and strongly resembles the π^* state of isolated acetone (Fig. 7). This orbital may correspond to the LUMO of the overall system, LUMO+1 being a pure water state, as at $t\simeq 1.5$ ps (Fig. 7). Alternatively, the order of these two states can be reversed (e.g., at 2.1 ps), and the optically active π^* is pushed up to the LUMO+1 level. No hybridization is again observed between π^* and water states, in analogy with $(CH_3)_2CO\cdot(H_2O)_2$. The solvent partner in this doublet of empty states is of special interest. Similar virtual orbitals, detached from the conduction band, have been observed previously in *ab initio* simulations of pure liquid water.[82,83] These semilocalized states are stabilized by regions where the σ^* orbitals are optimally in-phase. However, the clear separation (~ 1.5 eV) between the lowest virtual state of clean water and higher energy states is an artifact of our calculations and should be attributed to finite-size effects: in the limit of very large simulation cells, progressive accumulation of Kohn–Sham states at the bottom of the conduction band would eventually yield a quasicontinuous EDOS plot even in this gap region.[84] (For an experimental view of the electronic states of liquid water see, e.g., Refs. 85 and 86.)

The electronic absorption spectrum computed from the 10 lowest excitations is shown in Fig. 8. The 3–4.4 eV region presents several broad low-intensity ($f\simeq 10^{-4}$) features, followed by an abrupt upturn in intensity at ~ 4.4 eV.

The resolution into partial spectra arising from subsets of transitions shows that the whole low-energy tail of the spectrum builds up exclusively from the lowest 4 or 5 excitations, and that $\omega_1(t)$ is the sole responsible for the lowest 3–4 eV region. The deconvolution into single-transition excitation partial spectra $F_I(\omega)$ according to Eq. (64) (lower half of Fig. 8) shows that the moderate increase in intensity in the intermediate 4–4.4 eV region is largely due to the high density of transitions with similar energy and comparable oscillator strengths ($\omega_2-\omega_5$). The contribution from ω_1 in this frequency interval is almost negligible. These intermediate-energy excitations exhibit oscillations of up to 0.6 eV, while ω_1 is spread out over a considerably larger range of $\sim$1.6 eV. The steep rise in intensity at $\sim$4.4−4.6 eV marks the threshold of the solvent→solvent transition region, and may be regarded as a lower bound for the TDDFT energy gap. This appears to be virtually unchanged with respect to the Kohn–Sham value of pure water [$E_g=4.6$ eV (Ref. 82)]. Available experimental estimates from various optical techniques are substantially higher [$E_g=8.40-10.06$ eV (Refs. 87–91)], with a most probable value of 8.7 ± 0.5 eV (Ref. 85). Although additional calculations on clean water would be required for a more precise estimate of the energy gap, our results remain indicative of the failure of TDDFT in predicting excitations in extended systems (for further discussion see the next section).

Our approach does nonetheless allow for a meaningful interpretation of the low energy region of the spectrum, where the $n\rightarrow\pi^*$ transition is most likely to be found. With respect to gas-phase $(CH_3)_2CO\cdot(H_2O)_2$, the assignment of a particular band in the spectrum to a well defined Kohn–Sham excitation is complicated by the energy oscillations in time of the n and π^* states close to the edge of the valence and conduction bands of water. The problem is however simplified by the nearly complete lack of hybridization between acetone and water orbitals. This makes it possible to trace a low-energy TDDFT excitation back to a particular Kohn–Sham transition, provided the nature of the Kohn–Sham states at the water band edges are known. We therefore performed a Kohn–Sham Hamiltonian diagonalization (including 2 virtual states) for several ionic configurations taken from the MD run and analyzed the resulting orbitals. In all situations we found the $n\rightarrow\pi^*$ transition to correspond either to the second or third lowest TDDFT excitations, much less frequently to the lowest one. This excitation, ω_1, was found to arise predominantly from a solute $(n)\rightarrow$solvent transition (HOMO→LUMO+1 in Fig. 7), while ω_4 and ω_5 were either solvent→solvent or solvent→solute (π^*) transitions.

Oscillator strengths for the $n\rightarrow\pi^*$ transition were computed in a typical range of $10^{-4}-10^{-3}$, with occasional maxima up to $\sim10^{-2}$. On the basis of our analysis of the spectrum, we determined the $n\rightarrow\pi^*$ transition energy from the composite ($\omega_2+\omega_3$) partial spectrum (Fig. 9). This gave $\omega_{2+3}=4.37$ eV, corresponding to a blueshift of 0.19 eV with respect to gas-phase acetone. We remark that, despite its excellent agreement with experiment, this value should be considered only as an approximate estimate of the $n\rightarrow\pi^*$ transition in solution, as a non-negligible number of spurious

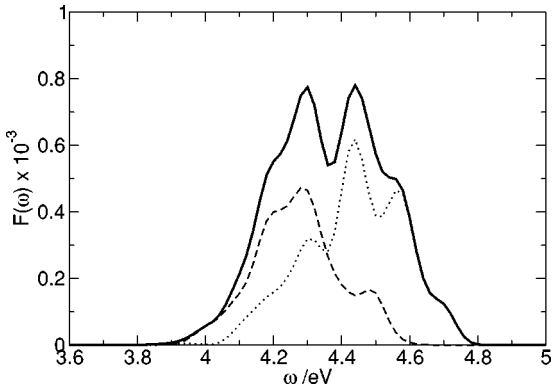

FIG. 9. Composite partial spectrum (solid line) obtained by adding the single-excitation spectra F_{ω_2} (dashed) and F_{ω_3} (dotted) of Fig. 8.

solvent→solute and solvent→solvent transitions are likely to be included in the composite spectrum. For the same reason, an accurate estimate of the overall intensity of the transition remains unavailable, though an overall gain in intensity of the $n\rightarrow\pi^*$ transition in solution with respect to the gas-phase molecule at the same temperature is evident.

VI. SUMMARY AND OUTLOOK

TDDFT calculations of the $n\rightarrow\pi^*$ excitation energy and oscillator strength in acetone, the gas-phase cluster $(CH_3)_2CO\cdot(H_2O)_2$ and acetone in water have been described. For the molecule, a shift of 0.27 eV was computed with respect to the time independent Kohn–Sham HOMO-LUMO energy difference, bringing this value in closer agreement with experiment and high-level *ab initio* calculations. Thermal excitation effects were found to be responsible for an increase in the oscillator strength up to $\sim10^{-4}$ at $T=298$ K. In the gas-phase cluster, three low energy weakly-allowed transitions were identified, arising from the near degeneracy of the three nonbonding (n) orbitals of solute and solvent. This system was studied at low temperature (25 K), and transition energies and oscillator strengths were computed, only slightly modified by the thermal motion. The highest-energy transition was found to be much more sensitive to adjustment by TDDFT compared to the two lower frequency lines. For this third transition energy a blueshift of 0.17 eV with respect to acetone was obtained. The two other lines were assigned to solvent→solute charge transfer, and, in view of the deficiency of TDDFT in accounting for excitations involving transfer of electrons over large (~1 Å) distances, we argued that these bands should not have been there at all.

The purpose of the hydrated cluster computation was mainly validation and help for the interpretation of the spectrum in solution. The near degeneracy of the nonbonding orbitals of solvent and solute translated to an electronic structure in solution with the n orbital of acetone near or at the edge of the valence band. As a result the same spurious solvent→solute charge transfer excitations persist in solution, overlapping with the physical transition form the nonbonding state of the solute. The solution, however, also exhibited a second type of charge transfer excitation, not seen

in the cluster, namely a solute→solvent transition. This transition is the consequence of an effective degeneracy of the acetone π^* orbital and the delocalized LUMO of the solvent. The n and π^* state of the solute, together with this one virtual solvent state and at most two other occupied nonbonding water orbitals, are responsible for the low intensity features in the calculated electronic excitation spectrum below the threshold of the solvent→solvent excitations. By analysing the nature of the Kohn–Sham orbitals involved in turn in each TDDFT transition, we were able to estimate a most probable value for the solvent shift of ~0.19 eV, consistent with experimental findings. The average intensity of the $n\rightarrow\pi^*$ transition was also found to be enhanced with respect to gas-phase acetone at the same temperature.

We regard this success, confirming a result already obtained in the QM/MM calculation of Ref. 36, of less significance than the failures uncovered in this investigation. These failures can be traced back to familiar deficiencies in the GGA/ALDA implementation employed in our calculation. The adverse effects, however, are amplified in aqueous acetone by critical degeneracies in both occupied and empty one-electron energy levels. The optically active π^* state was found at the same energy as the LUMO of the solvent. Of these two levels the energy of the π^* must be considered the most trustworthy since this localized molecular state is hardly affected by solvent effects. On the other hand, energy gaps in the density of states of extended systems tend to be underestimated by several eV and liquid water is no exception. The coincidence with the acetone π^* is therefore most likely accidental. The unfortunate consequence, however, is a false resonance between the $n\rightarrow\pi^*$ transition and solute →solvent charge transfer transitions. These interactions will be automatically eliminated if we succeed in increasing the gap in the pure solvent spectrum. The problem of the solute→solvent charge transfer seems to reduce, therefore, to the well known band gap problem of DFT. Several schemes have been proposed to address this problem, mostly with application to semiconductors in mind. Some of these methods involve improvement of the response kernel, e.g., by introducing self-interaction corrections[20] or a dependence on frequency and current.[29] Other approaches focus on enlarging the energy separation between the static KS energies by including exact exchange[92,93] or other forms of orbital dependence.[28,94]

The degeneracy of carbonyl and solvent HOMO, in contrast, is not accidental but a fundamental feature of the chemistry of this functional group. Adjustment of the static KS eigenvalues may improve the transition frequencies but will not eliminate the interference with solvent→solute charge transfers, which must be resolved at the level of the response kernel. This point is strongly supported by the analysis of Dreuw *et al.*[24] emphasizing the vital contribution of exact exchange in the response kernel. It remains to be seen whether the problem can be solved by the new kernels that have been proposed.[20,29] It is, however, this fundamental issue of charge transfer between molecules or across large molecules that stands in the way of the application of TDDFT to more complex systems..[22–24] With the present investigation of the electronic absorption spectrum of aqueous acetone, we hope to have demonstrated that this classic model system in computational chemistry continues to be relevant for testing methods in TDDFT. For more on the Berry phase polarization approach to the time dependent (non-adiabatic) regime see I. Souza, J. Ineguez, and D. Vanderbilt (ArXiv:cond-mat/0309259 v1, submitted to Phys. Rev. B).

ACKNOWLEDGMENTS

The research reported here is part of the 2001–2004 CCCP1 flagship project supported by EPSRC, which also sponsored the PDRA position of L.B. The calculations were performed on the Beowulf cluster of the Computational Science and Engineering Department at the Daresbury Laboratories of the CLRC. We are grateful for the helpful discussions with Nicholas Handy and Nikos Doltsinis.

APPENDIX: PROOF OF EQ. (16)

To determine the time derivative of the polarization $\mathbf{P}$ as defined in Eq. (10), we express $\mathbf{P}$ in terms of a sum of expectation values of the position operator with respect to to the one-electron orbitals

$$\mathbf{P}=-\frac{2e}{L^3}\sum_{n=1}^{\mathrm{occ}}\int d\mathbf{r}\phi_n^*\mathbf{r}\phi_n$$

which enables us to exploit the time dependent KS equations

$$\dot{\mathbf{P}}=-\frac{2e}{L^3}\sum_{n=1}^{\mathrm{occ}}\int d\mathbf{r}\left(\frac{\partial\phi_n^*}{\partial t}\mathbf{r}\phi_n+\phi_n^*\mathbf{r}\frac{\partial\phi_n}{\partial t}\right)$$

$$=-\frac{2ie}{\hbar L^3}\sum_{n=1}^{\mathrm{occ}}\int d\mathbf{r}\phi_n^*[H,\mathbf{r}]\phi_n. \tag{A1}$$

The commutator is easily evaluated using product rules

$$[H,\mathbf{r}]=\frac{1}{2m}\left[\left(\mathbf{p}+\frac{e}{c}\mathbf{A}\right)^2+V_{\mathrm{eff}}(\mathbf{r}),\mathbf{r}\right]$$

$$=\frac{1}{2m}\left(\left(\mathbf{p}+\frac{e}{c}\mathbf{A}\right)\left[\mathbf{p}+\frac{e}{c}\mathbf{A},\mathbf{r}\right]+\left[\mathbf{p}+\frac{e}{c}\mathbf{A},\mathbf{r}\right]\left(\mathbf{p}+\frac{e}{c}\mathbf{A}\right)\right)$$

$$=\frac{1}{2m}\left(\left(\mathbf{p}+\frac{e}{c}\mathbf{A}\right)[\mathbf{p},\mathbf{r}]+[\mathbf{p},\mathbf{r}]\left(\mathbf{p}+\frac{e}{c}\mathbf{A}\right)\right)$$

$$=\frac{\hbar}{mi}\left(\mathbf{p}+\frac{e}{c}\mathbf{A}\right).$$

Substituting in Eq. (A1) we obtain $\dot{\mathbf{P}}=\mathbf{J}$ with the current $\mathbf{J}$ given by Eq. (14).

We have been unable to repeat this derivation with $\mathbf{P}$ replaced by the Berry phase expression Eq. (20) for the dynamical polarization. (See, however, Ref. 43 for a related proof of the hypervirial theorem.) However, Eq. (20) is the Γ point approximation[40,41] to the original reciprocal space expression of King-Smith and Vanderbilt,[38,39] computed from an integral over the first Brillouin zone (BZ),

$$\mathbf{P}=-\frac{2ei}{(2\pi L)^3}\sum_{n=1}^{\text{occ}}\int_{\text{BZ}}d\mathbf{q}\langle u_{n\mathbf{q}}|\nabla_{\mathbf{q}}u_{n\mathbf{q}}\rangle, \tag{A2}$$

where $\mathbf{q}$ is the crystal momentum quantum number. $u_{n\mathbf{q}}(\mathbf{r})$ is the periodic part of the corresponding Bloch function

$$\phi_{n\mathbf{q}}(\mathbf{r})=e^{i\mathbf{q}\cdot\mathbf{r}}u_{n\mathbf{q}}(\mathbf{r}) \tag{A3}$$

with normalization

$$\frac{1}{L^3}\int_{\text{cell}}d\mathbf{r}|u_{n\mathbf{q}}(\mathbf{r})|^2=1,$$

where n is a band index. The generalization of the proof above for the reciprocal space expression Eq. (A2) is relatively straightforward. The key is the form of the Hamiltonian $H(\mathbf{q})$ controlling the motion of $u_{n\mathbf{q}}(\mathbf{r})$. By substitution of Eq. (A3) in the KS equation, we find

$$H(\mathbf{q})=\frac{1}{2m}\left(\mathbf{p}+\hbar\mathbf{q}+\frac{e}{c}\mathbf{A}\right)^2+V_{\text{eff}}(\mathbf{r}).$$

As before, taking the time derivative of Eq. (A2) leads to the expectation value of a commutator involving $H(\mathbf{q})$,

$$\dot{\mathbf{P}}=\frac{2e}{\hbar(2\pi L)^3}\sum_{n=1}^{\text{occ}}\int_{\text{BZ}}d\mathbf{q}\int_{\text{cell}}d\mathbf{r}\,u_{n\mathbf{q}}^*[H(\mathbf{q}),\nabla_{\mathbf{q}}]u_{n\mathbf{q}}. \tag{A4}$$

Working out the commutator with the derivative with respect to wave vector $\mathbf{q}$ gives

$$[H(\mathbf{q}),\nabla_{\mathbf{q}}]=-\frac{\hbar}{m}\left(\mathbf{p}+\hbar\mathbf{q}+\frac{e}{c}\mathbf{A}\right).$$

Inserting in Eq. (A4) we obtain, using Eq. (A3),

$$\mathbf{P}=-\frac{2e}{m(2\pi L)^3}\sum_{n=1}^{\text{occ}}\int_{\text{BZ}}d\mathbf{q}\langle u_{n\mathbf{q}}|\mathbf{p}+\hbar\mathbf{q}+\frac{e}{c}\mathbf{A}|u_{n\mathbf{q}}\rangle$$

$$=-\frac{2e}{m(2\pi L)^3}\sum_{n=1}^{\text{occ}}\int_{\text{BZ}}d\mathbf{q}\langle\phi_{n\mathbf{q}}|\mathbf{p}+\frac{e}{c}\mathbf{A}|\phi_{n\mathbf{q}}\rangle$$

in which we recognize the full reciprocal space expansion of the current. Restricting the k space summation to the central k point gives Eq. (14).

[1] E. Runge and E. K. U. Gross, Phys. Rev. Lett. **52**, 997 (1984).
[2] E. K. U. Gross, J. F. Dobson, and M. Petersilka, in *Density Functional Theory*, Springer Series in Topics in Current Chemistry, edited by R. F. Nalewajski (Springer, Heidelberg, 1996), Vol. 181.
[3] M. E. Casida, in *Recent Developments and Applications of Modern Density Functional Theory*, Theoretical and Computational Chemistry, edited by J. M. Seminario (Elsevier, Amsterdam, 1996), Vol. 4.
[4] C. Jamorski, M. E. Casida, and D. R. Salahub, J. Chem. Phys. **104**, 5134 (1996).
[5] S. J. A. Gisbergen, J. G. Snijders, and E. J. Baerends, J. Chem. Phys. **103**, 9347 (1996).
[6] R. Bauernschmitt and R. Ahlrichs, Chem. Phys. Lett. **256**, 454 (1996).
[7] K. B. Wiberg, R. E. Stratmann, and M. J. Frisch, Chem. Phys. Lett. **297**, 60 (1998).
[8] R. E. Stratmann, G. E. Scuseria, and M. J. Frisch, J. Chem. Phys. **109**, 8218 (1998).
[9] A. Görling, H. H. Heinze, S. Ph. Ruzankin, M. Staufer, and N. Rösch, J. Chem. Phys. **110**, 2785 (1999).
[10] N. L. Doltsinis and M. Sprik, Chem. Phys. Lett. **330**, 563 (2000).
[11] J. Hutter, J. Chem. Phys. **118**, 3928 (2003).
[12] R. Car and M. Parrinello, Phys. Rev. Lett. **55**, 2471 (1985).
[13] D. Marx and J. Hutter, *Ab Initio Molecular Dynamics: Theory and Implementation*, Vol. 1, in *Modern Methods and Algorithms of Quantum Chemistry*, edited by J. Grotendorst (2000), p. 301.
[14] C. Van Caillie and R. D. Amos, Chem. Phys. Lett. **308**, 249 (1999).
[15] C. Van Caillie and R. D. Amos, Chem. Phys. Lett. **317**, 159 (2000).
[16] F. Furche and R. Ahlrichs, J. Chem. Phys. **117**, 7433 (2002).
[17] R. D. Amos, Chem. Phys. Lett. **364**, 612 (2002).
[18] A. Dal Corso, F. Mauri, and A. Rubio, Phys. Rev. B **53**, 15638 (1996).
[19] F. Kootstra, P. L. Boeij, and J. G. Snijders, J. Chem. Phys. **112**, 6517 (2000).
[20] L. Reining, V. Olevano, A. Rubio, G. Onida, and L. Reining, Phys. Rev. Lett. **88**, 066404 (2002).
[21] G. Onida, L. Reining, and A. Rubio, Rev. Mod. Phys. **74**, 601 (2002).
[22] D. J. Tozer, R. D. Amos, N. C. Handy, B. O. Roos, and L. Serrano-Andres, Mol. Phys. **97**, 859 (1999).
[23] C. Zheng-Li, K. Sendt, and J. R. Reimers, J. Chem. Phys. **117**, 5543 (2002).
[24] A. Dreuw, J. L. Weisman, and M. Head-Gordon, J. Chem. Phys. **119**, 2943 (2003).
[25] M. E. Casida, F. Gutierez, J. Guan, F.-X. Gadea, D. Salahub, and J.-P. Daudey, J. Chem. Phys. **113**, 7062 (2000).
[26] O. V. Gritsenko, S. J. A. van Gisbergen, A. Görling, and E. J. Baerends, J. Chem. Phys. **113**, 8478 (2000).
[27] S. J. A. Gisbergen, P. R. T. Schippers, O. V. Gritsenko, E. J. Baerends, J. G. Snijders, B. Champagne, and B. Kirtman, Phys. Rev. Lett. **83**, 694 (1999).
[28] M. Grüning, O. V. Gritsenko, and E. J. Baerends, J. Chem. Phys. **116**, 6435 (2002).
[29] M. van Faassen, P. L. Boeij, R. van Leeuwen, J. A. Berger, and J. G. Snijders, Phys. Rev. Lett. **88**, 186401 (2002); J. Chem. Phys. **112**, 6517 (2000).
[30] M. Karelson and M. C. Zerner, J. Am. Chem. Soc. **112**, 9405 (1990).
[31] M. Karelson and M. C. Zerner, J. Phys. Chem. **96**, 6949 (1992).
[32] J. T. Blair, K. Krogh-Jespersen, and R. M. Levy, J. Am. Chem. Soc. **111**, 6948 (1989).
[33] R. M. Levy, D. B. Kitchen, J. T. Blair, and K. Krogh-Jespersen, J. Phys. Chem. **94**, 4470 (1990).
[34] N. A. Besley and J. D. Hirst, J. Phys. Chem. A **102**, 10791 (1998).
[35] M. L. Sánchez, M. E. Martín, M. A. Aguilar, and F. J. Olivares del Valle, Chem. Phys. Lett. **310**, 195 (1999).
[36] U. F. Röhrig, I. Frank, J. Hutter, A. Laio, J. VandeVondele, and U. Röthlisberger, Chem. Phys. Chem. (in press).
[37] C. Reichard, *Solvents and Solvent Effects in Organic Chemistry* (VCH Verlaggesellschaft mbH, Weinheim, 1988).
[38] R. D. King-Smith and D. Vanderbilt, Phys. Rev. B **47**, 1651 (1993).
[39] D. Vanderbilt and R. D. King-Smith, Phys. Rev. B **48**, 4442 (1993).
[40] R. Resta, Rev. Mod. Phys. **66**, 899 (1994).
[41] R. Resta, Phys. Rev. Lett. **80**, 1800 (1998).
[42] R. Resta and S. Sorella, Phys. Rev. Lett. **82**, 370 (1999).
[43] I. Souza, T. Wilkens, and R. M. Martin, Phys. Rev. B **62**, 1666 (2000).
[44] M. Merchan, B. O. Roos, R. McDiarmid, and X. J. Xing, J. Chem. Phys. **104**, 1791 (1996).
[45] K. N. Walzl, C. F. Koerting, and A. J. Kuppermann, J. Chem. Phys. **87**, 3796 (1987).
[46] B. Hess, P. J. Bruna, R. J. Buenker, and S. D. Peyerimhoff, Chem. Phys. **18**, 267 (1976).
[47] S. R. Gwaltney and R. J. Bartlett, Chem. Phys. Lett. **241**, 26 (1995).
[48] M. Baba and I. Hanazaki, Chem. Phys. Lett. **103**, 93 (1983).
[49] N. S. Bayliss and E. G. McRae, J. Phys. Chem. **58**, 1006 (1954).
[50] A. Balasubramanian and C. N. R. Rao, Spectrochim. Acta **18**, 1337 (1962).
[51] W. P. Hayes and C. C. Name, Spectrochim. Acta **21**, 529 (1965).
[52] N. S. Bayliss and G. Wills-Johnson, Spectrochim. Acta, Part A **24**, 551 (1968).
[53] D.-W. Liao, A. M. Mebel, Y.-T. Chen, and S.-H. Lin, J. Phys. Chem. A **101**, 9925 (1997).
[54] I. Frank, J. Hutter, D. Marx, and M. Parrinello, J. Chem. Phys. **108**, 4060 (1998).
[55] R. Loudon, *The Quantum Theory of Light* (Clarendon, Oxford, 1973).
[56] S. K. Gosh and A. K. Dhara, Phys. Rev. A **38**, 1149 (1988).
[57] A. J. Stone, *The Theory of Intermolecular Forces* (Clarendon, Oxford, 1996).
[58] G. Berghold, C. J. Mundy, A. H. Romero, J. Hutter, and M. Parrinello, Phys. Rev. B **61**, 10040 (2000).

[59] P. L. Silvestrelli, M. Bernasconi, and M. Parrinello, Chem. Phys. Lett. **277**, 478 (1997).
[60] M.-P. Gaigeot and M. Sprik, J. Phys. Chem. B (in press).
[61] A. Putrino and M. Parrinello, Phys. Rev. Lett. **88**, 176401 (2002).
[62] A. L. Fetter and J. D. Walecka, *Quantum Theory of Many-Particle Systems* (McGraw–Hill, New York, 1971).
[63] S. Hirata and M. Head-Gordon, Chem. Phys. Lett. **302**, 375 (1999).
[64] S. Hirata and M. Head-Gordon, Chem. Phys. Lett. **314**, 291 (1999).
[65] A. Putrino, D. Sebastiani, and M. Parrinello, J. Chem. Phys. **113**, 7102 (2000).
[66] CPMD, Version 3.6, J. Hutter *et al.*, Copyright MPI für Festkörperforschung Stuttgart 1997–2001; see also www.cpmd.org.
[67] S. Goedecker, M. Teter, and J. Hutter, Phys. Rev. B **54**, 1703 (1996).
[68] N. Troullier and J. L. Martins, Phys. Rev. B **43**, 1993 (1991).
[69] A. Becke, Phys. Rev. A **38**, 3098 (1988).
[70] C. Lee, W. Yang, and R. G. Parr, Phys. Rev. B **37**, 785 (1988).
[71] R. Bauernschmitt, M. Häser, O. Treutler, and R. Ahlrichs, Chem. Phys. Lett. **256**, 454 (1996).
[72] E. R. Davidson, J. Comput. Phys. **17**, 87 (1975).
[73] K. B. Wiberg, C. M. Hadad, J. B. Foresman, and W. A. Chupka, J. Phys. Chem. **96**, 10756 (1992).
[74] W.-C. Tam and C. E. Brion, J. Electron Spectrosc. Relat. Phenom. **4**, 139 (1974).
[75] W. M. St. John, III, R. C. Estler, and J. P. Doering, J. Chem. Phys. **61**, 673 (1974).
[76] A. B. Rocha and C. E. Bielschowsky, Chem. Phys. Lett. **337**, 331 (2001).
[77] J. Del Bene, J. Am. Chem. Soc. **96**, 5644 (1974).
[78] J. Del Bene, J. Am. Chem. Soc. **95**, 6517 (1973).
[79] Y. Dimitrova and S. D. Peyerimhoff, J. Phys. Chem. **97**, 12731 (1993).
[80] D. S. Venables and C. A. Schmuttenmaer, J. Chem. Phys. **113**, 3249 (2000).
[81] P. Hunt, M. Sprik, and R. Vuilleumier, Chem. Phys. Lett. **376**, 68 (2003).
[82] K. Laasonen, M. Sprik, M. Parrinello, and R. Car, J. Chem. Phys. **99**, 9080 (1993).
[83] M. Boero, M. Parrinello, K. Terakura, T. Ikeshoji, and C. C. Liew, Phys. Rev. Lett. **90**, 226403 (2003).
[84] J. VandeVondele and M. Sprik (unpublished).
[85] A. Bernas, C. Ferradini, and J.-P. Jay-Gerin, Chem. Phys. **222**, 151 (1997).
[86] A. Bernas, C. Ferradini, and J.-P. Gerin, J. Photochem. Photobiol., A **117**, 171 (1998).
[87] I. Watanabe, J. B. Flanagan, and P. Delahay, J. Chem. Phys. **73**, 2057 (1980).
[88] T. Watanabe and H. Gerischer, J. Electroanal. Chem. Interfacial Electrochem. **122**, 73 (1981).
[89] P. Delahay and K. von Burg, Chem. Phys. Lett. **83**, 250 (1981).
[90] P. Delahay, Acc. Chem. Res. **15**, 40 (1982).
[91] W. Grevendonk, J. Dauwen, P. Van den Keybus, and B. Vanhuyse, J. Chem. Phys. **81**, 3746 (1984).
[92] D. M. Bylander and L. Kleinman, Phys. Rev. B **52**, 14566 (1995).
[93] M. Städele, J. A. Majewski, P. Vogel, and A. Görling, Phys. Rev. Lett. **79**, 2089 (1997).
[94] P. R. T. Schipper, O. V. Gritsenko, S. J. A. van Gisbergen, and E. J. Baerends, J. Chem. Phys. **112**, 1344 (2000).